Optics Letters

Nonlinear pulse compression in a gas-filled multipass cell

Moritz Ueffing,[1,*] Simon Reiger,[1] Martin Kaumanns,[1] Vladimir Pervak,[1] Michael Trubetskov,[2] Thomas Nubbemeyer,[1] and Ferenc Krausz[1,2]

[1]Ludwig-Maximilians-Universität München, Am Coulombwall 1, 85748 Garching, Germany
[2]Max-Planck-Institut für Quantenoptik, Hans-Kopfermann-Str. 1, 85748 Garching, Germany
*Corresponding author: moritz.ueffing@mpq.mpg.de

Received 8 February 2018; accepted 24 March 2018; posted 28 March 2018 (Doc. ID 322807); published 24 April 2018

We present an efficient method for compressing sub-picosecond pulses at 200 W average power with 2 mJ pulse energy in a multipass cell filled with different gases. We demonstrate spectral broadening by more than a factor of five using neon, argon, and nitrogen as nonlinear media. The 210 fs input pulses are compressed down to 37 fs and 35 GW peak power with a beam quality factor of 1.3 × 1.5 at a power throughput of >93%. This concept represents an excellent alternative to hollow-core fiber-based compression schemes and optical parametric amplifiers (OPAs).

OCIS codes: (140.7090) Ultrafast lasers; (190.7110) Ultrafast nonlinear optics; (320.5520) Pulse compression; (320.7110) Ultrafast nonlinear optics.

https://doi.org/10.1364/OL.43.002070

Nonlinear pulse compression constitutes a key technology to reduce the pulse duration of laser systems well below the gain bandwidth limitation of the underlying laser gain medium. For more than a decade compressed few-cycle pulses emitted from titanium sapphire (Ti:sa) lasers [1–3] have enabled time-resolved metrology in the attosecond time domain [4]. Ti:sa lasers provide up to ∼50 W average power and multi-millijoule pulse energies. However, the average power scaling of Ti:sa lasers is challenging, which restricts the available repetition rate of multi-millijoule Ti:sa laser amplifiers to the kilohertz regime. With the increasing progress in the field of attosecond science, this limitation gains significance as it prevents fast data acquisition and hinders the investigation of rare events, such as coincident measurements [5].

To this end, there exist two paths to generate high-power few-cycle laser pulses with high repetition rates. The first is based on direct amplification of ultra-broadband laser pulses in optical parametric amplifier (OPA) systems. These systems reach outstanding performance [6,7]; however, the low energy conversion efficiency necessitates sophisticated pump laser architectures that increase the overall cost and complexity of the system. The second approach implements pulse compression schemes to reduce the pulse duration of the gain bandwidth limited laser pulses. In these systems, higher efficiencies are reached if losses in the pulse compression setup are minimized. Today, state-of-the-art Yb-doped laser materials provide pulse durations between ∼100 fs and 10 ps at kilowatt average power in Innoslab [8], fiber [9], and thin-disk geometries [10,11]. The major challenge in generating few-cycle laser pulses from these sources lies in the efficient compression of the hundreds of watt average power and pulse energies of several tens of millijoules.

Pulse compression in hollow-core fibers [1] has been successfully demonstrated with good beam parameters, more than 650 W average power [12] and 8 mJ pulse energy [13], providing one of the best tools for few-cycle pulse generation so far. However, laboratory space and the lack of long capillaries impose limitations in energy scaling [13]. Furthermore, hollow-core fibers are prone to optical damage in case of misalignment, which becomes increasingly critical for high average power laser systems. Recently, alternative compression schemes based on distributed spectral broadening in bulk media forgoing the hollow-core fiber have been demonstrated [14–16]. This technique yields good conversion efficiency and high compression ratios of almost a factor of 10, and maintains the beam quality to good extent. Distributed spectral pulse compression is demonstrated for systems with microjoule pulse energies at the megawatt [15,16] and the gigawatt [14] peak power level. However, aiming for a pulse compression scheme that supports millijoule pulse energies with peak powers of several gigawatts, a multipass cell based on bulk would significantly grow in size and prevents a compact setup.

Therefore, we report on a nonlinear compression setup based on a gas-filled multipass cell [17–19]. We show data for neon, argon, and nitrogen depending on the gas pressure and demonstrate compression of the 2 mJ, 210 fs input pulses to 37 fs with 35 GW peak power in argon while maintaining excellent beam parameters. The setup is fully scalable in pulse energy and average power by choosing different gases, pressures, and focal lengths of the imaging mirrors. Being based purely on high-reflective optics, the concept provides the possibility for dispersion control during the nonlinear processes and; in contrast to hollow-core fibers, the risk of optical damage

is strongly reduced. Additionally, the design of the multipass cell facilitates the adjustment of the beam diameter to avoid any ionization effects and, because of the imaging system, the concept is simple to align. This approach could enable compression to the few-cycle regime with kilowatt average powers, pulse energies exceeding tens of millijoules, and provides a much more efficient alternative to OPAs.

The setup is based on an all-nonlinear approach starting with a nonlinear regenerative Yb:YAG thin-disk amplifier described in [20]. The amplifier emits 210 fs pulses after compression carrying 2 mJ pulse energy at a 100 kHz repetition rate corresponding to 200 W average power. The pulse-to-pulse RMS stability of the system is <0.5%, and the peak power of the pulses amounts to 7.3 GW. After the chirped mirror compressor, the laser beam passes a half-wave plate and a thin-film polarizer, allowing power adjustment and control of the intensity inside the multipass system.

Within the 4f imaging multipass cell, the beam propagates in three dimensions through the optical setup [Fig. 1(a)]. The setup incorporates four concave mirrors (MC1-MC4) with a radius of curvature of 1 m separated by 1 m. The concave mirrors have a size of 140 mm × 40 mm supporting enough aperture to guide the 3.2 mm ($1/e^2$) beam up to 14 times over a single mirror. Three 1 inch mirrors (MI1-MI3) are located at the imaging planes in 0.5 m distance from the curved optics. Tilting one of these mirrors increases or decreases the number of passes through the multipass cell. Additionally, two mirrors with apertures of 100 mm × 30 mm (MF1, MF2) are folding the beam, pulling the left and right imaging planes apart.

A single concave mirror with 3 m radius of curvature at the beginning of the system suffices to couple the beam to the multipass cell. This mirror focuses the beam and locates the beam waist in the middle between the concave imaging mirrors [Fig. 1(a), dashed lines]. Figure 1(b) shows the beam caustic for a full pass through the multipass cell, yielding 16 reflections on the high-reflective multilayer optics and four foci. In total, the multipass cell was operated with 6 iterations leading to 26 foci, including the two foci arising from in- and out-coupling.

With this setup, we compressed the 210 fs pulses of the nonlinear regenerative amplifier to 37 fs (FWHM) at 265 mbar gas pressure in argon corresponding to a compression ratio of 5.6 and a peak power of 35 GW. The chirp after the multipass cell is removed with a chirped mirror compressor consisting of four mirrors that have a group delay dispersion (GDD) of –2800 fs^2 in total. The main pulse contains 80% of the energy, as compared to the Fourier-limited pulse [Fig. 2]. The power throughput the nonlinear broadening process amounts to >93%, and the pulse-to-pulse stability of the output pulses is with an RMS value of <1% for $18 \cdot 10^3$ pulses which is well suited for further nonlinear processes.

Starting from an input M^2 of 1.12(X) and 1.15(Y), the beam quality factor shows a good behavior after the multipass cell, even for large nonlinear phase shifts. Figure 3 shows the measurement of the 192 W output beam at 265 mbar argon pressure. We observe a linear increase of the beam quality factor [Fig. 3, inset] to values between 1.3(X) and 1.5(Y) at maximum powers. Compared to the M^2 values under vacuum conditions with 1.2(X) and 1.3(Y), the beam quality reduces more strongly in the y- than in the x-direction. We attribute the different behavior of the two axes to differences in the nonlinear processes caused by the astigmatism of the multipass cell and the differences of the input beam quality factors.

The spectral homogeneity of the beam was characterized by measuring the spectrum across the x- and y-direction with an optical spectrum analyzer. The ~15 mm beam was scanned in

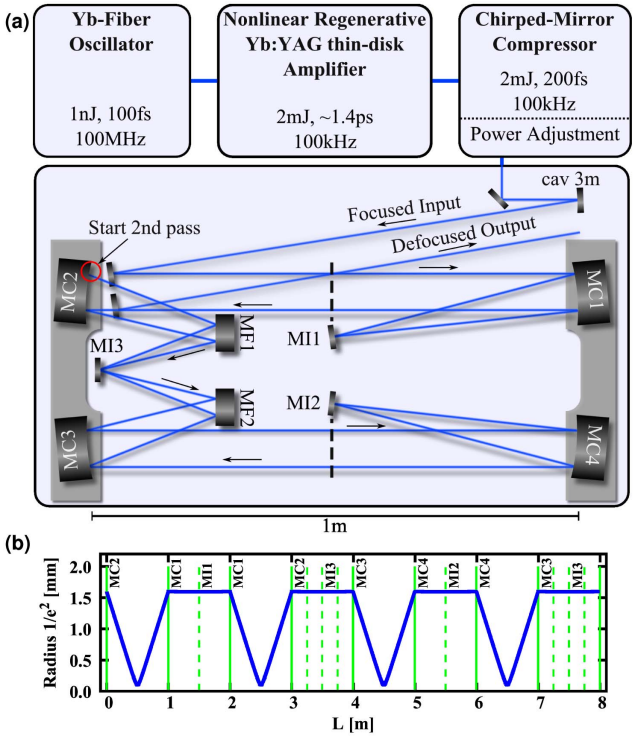

Fig. 1. (a) Nonlinear compression setup containing a nonlinear regenerative amplifier and the 4f imaging gas-filled multipass cell. MC, concave high reflectors with 1 m radius of curvature; MF, folding mirrors, flat; MI, mirrors in the imaging planes, flat. All mirrors possess a GDD of <10 fs^2. (b) Beam caustic for one round-trip through the multipass cell. The solid vertical lines illustrate the position of the concave 1 m imaging mirrors. The dashed vertical lines mark the positions of flat optics.

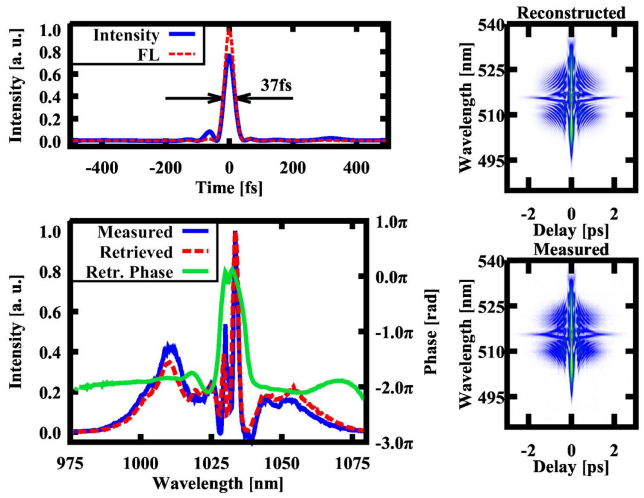

Fig. 2. Second-harmonic FROG measurement of the output pulse (G-error: 0.3%) at 265 mbar in argon and 1.9 mJ output energy. Upper left, Fourier-limited (FL, dashed) and retrieved pulse (solid). Lower left, measured spectrum, retrieved spectrum, and retrieved spectral phase.

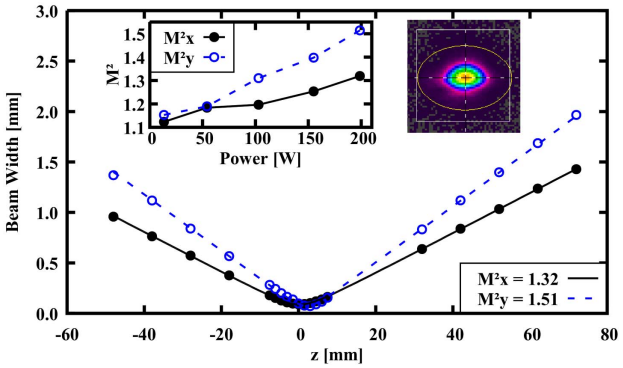

Fig. 3. Measurement of the beam quality factor (M^2) at 200 W input power and 265 mbar argon pressure. Insets, M^2 parameter depending on the input power and the beam profile in the focus ($z = 0$).

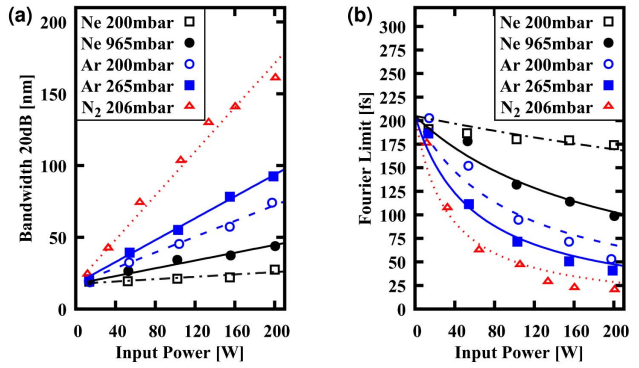

Fig. 4. (a) 20 dB spectral for different pressures of neon, argon, and nitrogen. (b) Corresponding calculated Fourier limits. The dashed and solid lines represent fitted linear (a) and the inverse function to the data points.

1 mm steps, and fractions of 0.5 mm were coupled into a single mode fiber. The homogeneity is characterized according to the definition $V_{x,y} := [\int \sqrt{I(\lambda) I_0(\lambda)} \mathrm{d}\lambda]^2 / [\int I(\lambda) \mathrm{d}\lambda \cdot \int I_0(\lambda) \mathrm{d}\lambda]$ [16], where $I(\lambda)$ is the spectrum of a single step, and $I_0(\lambda)$ is the reference spectrum at maximum intensity of the beam. The value of V_x drop to 89% within a ($\sim 1/e^2$) of the beam profile. In the outermost part of the beam ($I < 1/e^2$) V_x reduces to 56%. In the y-direction, we do not observe a reduction, and V_y remains larger than 92%. The intensity weighted averages are $V_x = 97.6\%$ and $V_y = 98.6\%$, reflecting good spectral homogeneity of the output beam.

The input intensity in the focal plane for the first pass was characterized by measuring the beam caustic with a beam profiler behind the concave 3 m mirror. From the data, we calculate the peak intensity to 60 TW/cm^2 and measure a focus $1/e^2$-diameter of 200 μm with 3.2 mm spot sizes on the curved optic (MC1) in the first pass. The fluences on the mirrors are then 0.05 J/cm^2, which is well below the damage threshold (~1 J/cm^2) of employed optics.

Gases at normal pressure exhibit nonlinear refractive indices of 0.6 μm^2/TW (He) [21,22], 1.4 μm^2/TW (Ne) [21,22], 17.4 μm^2/TW (Ar) [21,22], 20 μm^2/TW (Ar) [23], and 23 μm^2/TW (N_2) [24], leading to critical powers of >110 GW for neon, 9.2 GW for argon, and <7 GW for nitrogen. With 7.3 GW peak power of the driving laser gas, pressures below 1 bar for noble gases heavier than neon are necessary to avoid catastrophic self-focusing and damage of the multipass optics. To allow control of the gas pressure, a vacuum chamber embraces the whole setup. The design supports gas pressures between 10^{-2} mbar and normal pressure.

Figure 4 summarizes the measurements and illustrates the data at 200 mbar for neon, argon, and nitrogen. Figure 4(a) shows the output 20 dB spectral bandwidth, depending on the selected gases and the input power. Clearly, the process scales linearly with the pressure [21], indicating well-behaved beam profiles within the multipass cell. The calculated Fourier-limited pulse duration [Fig. 4(b)] reveals that neon supports only 100 fs pulses at normal pressure. As our setup only supports pressures up to ~1 bar, we required a gas with a higher nonlinear optical coefficient to reach a larger compression ratio. Nitrogen supports spectral bandwidths [Fig. 4(a)] exceeding the bandwidth for argon by a factor of 2.9 at same pressures and input powers. However, the output pulses lead to worse compression results after our chirped mirror compressor as compared to the results achieved with argon. We attribute the lowered performance to the slow rotational response of nitrogen [24,25] which leads to additional contributions from the Raman effect. Argon yields sufficient a spectral bandwidth to compress the pulse by a significant factor (>5), while keeping 80% of the energy in the main peak after compression. Both criteria could only be fulfilled with argon.

Pulse compression below the measured 37 fs by increasing the pressure of argon, in combination with fine tuning of the chirped mirror compressor, emerges difficult. Attempts to reduce the pulse duration at pressures above ~300 mbar led to pulses with less compression ratio and a significant amount of energy apart from the main peak. To understand the limitation of this process, we simulated the multipass configuration in a 2D split-step model, including the radial coordinate and the time coordinate. The data were then compared to the results from electric field measurements with a second-harmonic frequency-resolved optical gating (FROG) [Figs. 5(a) and 5(b)]. The simulated data are depicted in Figs. 5(c) and 5(d). Good agreement to the measured data are visible if the nonlinear refractive index at normal pressure is adjusted to 12 μm^2/TW, which is in good agreement with the literature values. Dispersion is introduced by both the high-reflective mirrors and by argon. The GDD of one high-reflective mirror amounts to ~8 fs^2, which contributes significantly due to the large number of bounces over these mirrors. The simulation shows the results using 8 fs^2 for each mirror and the dispersion for argon under normal pressure [26].

Figure 5(b) depicts the development of the pulse with increasing pressure. The instantaneous angular frequency [Fig. 5(b), solid] clearly shows the increasing amount of self-phase modulation (SPM) introduced to the pulse with increasing pressure. Additionally, the pulse shape alters and becomes rectangular. The latter is a well-known effect resulting from the combination of SPM and dispersion [27]. At pressures above 300 mbar, the pulse shows signs of optical wave breaking [27] leading to rapid oscillations [Fig. 5(b), top right] of the instantaneous angular frequency. Once the pulse reaches this limit, compression becomes difficult. Chirp management within the multipass cell, however, could facilitate pulse compression to 20 fs.

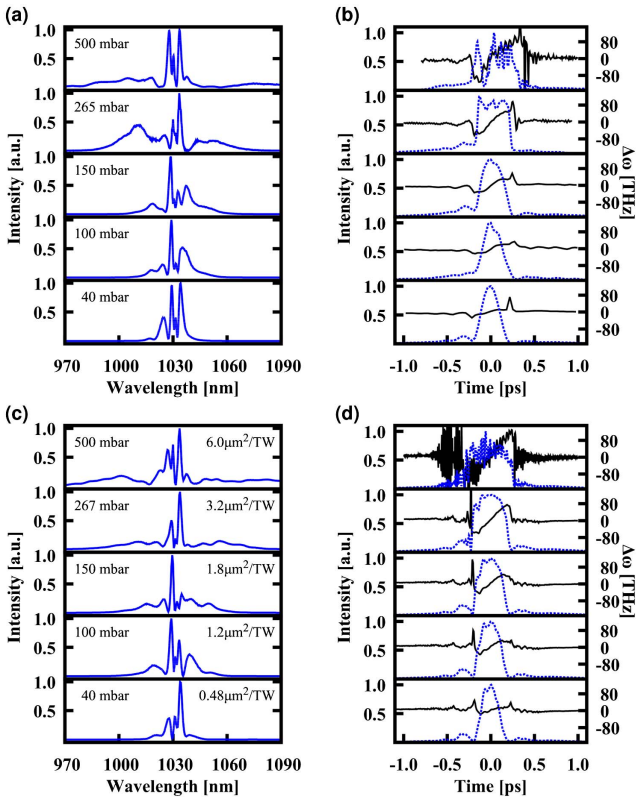

Fig. 5. (a) Measured spectra for argon and (b) measured pulse shape (dashed) and instantaneous angular frequency (solid) at 200 W input power. (c) Calculated spectra, (d) calculated pulse shape (dashed), and instantaneous angular frequency (solid). Horizontally aligned plots represent data at the same pressure and nonlinear refractive index [$n_2 = 12\ \mu m^2/TW(1\ bar)$].

Energy or intensity scaling of the compression scheme could be realized without the need for increasing the size of the setup in the first place. Due to the 4f imaging system, the input beam size is scalable and reduces the fluence on the mirror links to an increasing intensity in the focus of the multipass cell. Adjustment of the gas pressure to compensate for this effect is easily implemented. In the case of intensities permitting strong ionization of argon, neon and helium become suitable gas choices. For lower pulse energies, the system can be implemented using heavier noble gases such as krypton or xenon, allowing compression of pulses with energies <70 μJ (Xe, normal pressure). Implementation of pulse energies less than this value a high-pressure cell allows larger nonlinear optical coefficients.

In conclusion, we have presented a detailed experimental investigation of pulse compression based on a gas-filled multipass cell. The 210 fs input pulses have been spectrally broadened to a bandwidth of up to 90 nm (20 dB) in argon. We successfully compressed the pulses down to 37 fs at high-power throughputs of >93% at the full 200 W input power. Currently demonstrated peak powers and pulse durations are limited by the input power provided by the regenerative amplifier and by the use of simple, reflective non-dispersive optics inside the multipass cell. Further energy and average power scaling is feasible based already on the demonstrated design. Implementation of the dispersion compensation is another step towards generation of the few-cycle pulses.

Funding. Munich-Centre for Advanced Photonics (MAP).

Acknowledgment. The authors thank Oleg Pronin for his help in preparing this Letter. Furthermore, we acknowledge funding from the "Centre for Advanced Laser Applications."

REFERENCES

1. M. Nisoli, S. De Silvestri, and O. Svelto, Appl. Phys. Lett. **68**, 2793 (1996).
2. B. Schenkel, J. Biegert, U. Keller, C. Vozzi, M. Nisoli, G. Sansone, S. Stagira, S. De Silvestri, and O. Svelto, Opt. Lett. **28**, 1987 (2003).
3. A. L. Cavalieri, E. Goulielmakis, B. Horvath, W. Helml, M. Schultze, M. Fieß, V. Pervak, L. Veisz, V. S. Yakovlev, M. Uiberacker, A. Apolonski, F. Krausz, and R. Kienberger, New J. Phys. **9**, 242 (2007).
4. F. Krausz and M. Ivanov, Rev. Mod. Phys. **81**, 163 (2009).
5. G. Sansone, F. Kelkensberg, F. Morales, J. F. Perez-Torres, F. Martín, and M. J. J. Vrakking, IEEE J. Sel. Top. Quantum Electron. **18**, 520 (2012).
6. R. Budriūnas, T. Stanislauskas, J. Adamonis, A. Aleknavičius, G. Veitas, D. Gadonas, S. Balickas, A. Michailovas, and A. Varanavičius, Opt. Express **25**, 5797 (2017).
7. A. Vaupel, N. Bodnar, B. Webb, L. Shah, and M. Richardson, Opt. Eng. **53**, 051507 (2013).
8. P. Russbueldt, T. Mans, J. Weitenberg, H. D. Hoffmann, and R. Poprawe, Opt. Lett. **35**, 4169 (2010).
9. M. Müller, M. Kienel, A. Klenke, T. Gottschall, E. Shestaev, M. Plötner, J. Limpert, and A. Tünnermann, Opt. Lett. **41**, 3439 (2016).
10. J.-P. Negel, A. Loescher, A. Voss, D. Bauer, D. Sutter, A. Killi, M. A. Ahmed, and T. Graf, Opt. Express **23**, 21064 (2015).
11. T. Nubbemeyer, M. Kaumanns, M. Ueffing, M. Gorjan, A. Alismail, H. Fattahi, J. Brons, O. Pronin, H. G. Barros, Z. Major, T. Metzger, D. Sutter, and F. Krausz, Opt. Lett. **42**, 1381 (2017).
12. S. Hädrich, M. Kienel, M. Müller, A. Klenke, J. Rothhardt, R. Klas, T. Gottschall, T. Eidam, A. Drozdy, P. Jójárt, Z. Várallyay, E. Cormier, K. Osvay, A. Tünnermann, and J. Limpert, Opt. Lett. **41**, 4332 (2016).
13. F. Böhle, M. Kretschmar, A. Jullien, M. Kovacs, M. Miranda, R. Romero, H. Crespo, U. Morgner, P. Simon, R. Lopez-Martens, and T. Nagy, Laser Phys. Lett. **11**, 095401 (2014).
14. C.-H. Lu, Y.-J. Tsou, H.-Y. Chen, B.-H. Chen, Y.-C. Cheng, S.-D. Yang, M.-C. Chen, C.-C. Hsu, and A. H. Kung, Optica **1**, 400 (2014).
15. J. Schulte, T. Sartorius, J. Weitenberg, A. Vernaleken, and P. Russbueldt, Opt. Lett. **41**, 4511 (2016).
16. J. Weitenberg, A. Vernaleken, J. Schulte, A. Ozawa, T. Sartorius, V. Pervak, H.-D. Hoffmann, T. Udem, P. Russbüldt, and T. W. Hänsch, Opt. Express **25**, 20502 (2017).
17. N. Milosevic, G. Tempea, and T. Brabec, Opt. Lett. **25**, 672 (2000).
18. S. N. Vlasov, E. V. Koposova, and V. E. Yashin, Quantum Electron. **42**, 989 (2012).
19. M. Hanna, X. Délen, L. Lavenu, F. Guichard, Y. Zaouter, F. Druon, and P. Georges, J. Opt. Soc. Am. B **34**, 1340 (2017).
20. M. Ueffing, R. Lange, T. Pleyer, V. Pervak, T. Metzger, D. Sutter, Z. Major, T. Nubbemeyer, and F. Krausz, Opt. Lett. **41**, 3840 (2016).
21. D. P. Shelton, Phys. Rev. A **42**, 2578 (1990).
22. A. Couairon, H. S. Chakraborty, and M. B. Gaarde, Phys. Rev. A **77**, 023603 (2008).
23. V. Loriot, E. Hertz, O. Faucher, and B. Lavorel, Opt. Express **17**, 13429 (2009).
24. E. T. J. Nibbering, G. Grillon, M. A. Franco, B. S. Prade, and A. Mysyrowicz, J. Opt. Soc. Am. B **14**, 650 (1997).
25. V. Mizrahi and D. P. Shelton, Phys. Rev. Lett. **55**, 696 (1985).
26. E. R. Peck and D. J. Fisher, J. Opt. Soc. Am. **54**, 1362 (1964).
27. W. J. Tomlinson, R. H. Stolen, and A. M. Johnson, Opt. Lett. **10**, 457 (1985).